Appl. Math. and Comp. Sci., 1998, Vol.8, No.2, 213–251

ACTIVE NOISE AND VIBRATION CONTROL

STEPHEN J. ELLIOTT*

Active control can reduce sound and vibration by destructive interference between the original, primary, field and the field generated by controllable secondary sources. It is most effective at low frequencies, for which the wavelength of the disturbance is comparable with the dimensions of the region being controlled. In this review paper the physical limitations of performance are first explored for vibration on a plate and sound in an enclosure, and the nature of the plant response is discussed in these two cases. Adaptive feedforward control algorithms have been successfully used in active control, and these are discussed in terms of an equivalent feedback control system. Finally, the feedback control of sound and vibration is discussed, from the point of view of Internal Model Control, emphasising the importance of plant delay in determining optimal performance, and the trade-off between disturbance rejection and robust stability.

1. Introduction

Sound and vibration have conventionally been controlled using passive methods which involve absorbing the disturbance or blocking its transmission. These methods generally work well at high frequencies, where the wavelength of the disturbance is small compared with the structure or enclosure, but are less effective at low frequencies. At 100 Hz, for example, the wavelength of a soundwave under normal conditions in air is about 3.4 m, and it is difficult to absorb such a sound wave with a thin layer of absorbent material on the walls of an enclosure.

Active sound and vibration control exploits the long wavelengths associated with low frequency disturbances. It works on the principle of destructive interference between the original "primary" soundfield and that due to a number of controllable "secondary" sources. The secondary sources are generally adjusted to minimise the disturbance measured at a number of discrete sensors and a knowledge of the physics of the sound or vibration field is used to ensure that controlling the field at these points leads to attenuation over some useful region of the field. The main physical elements of an active control system are illustrated in Fig. 1, which shows a system acted upon by a number of primary and secondary sources. The signals driving the secondary sources are adjusted to minimise a cost function derived from measurements made on the system which can either give an indication of the system's global or local response.

* University of Southampton, Institute of Sound & Vibration Research, Highfield, Southampton SO17 1BJ, U.K., e-mail: sje@isvr.soton.ac.uk.

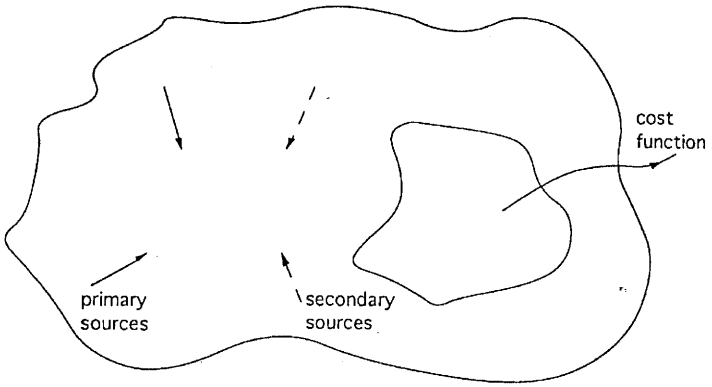

Fig. 1. The physical elements of an active control system.

Although the principle of active noise control dates back to 1936 (Lueg, 1936), and manually adaptive analogue control systems were developed in the 1950's (Conover, 1956), the modern era of active control was spurred by the availability of affordable DSP processors which allowed adaptive multichannel digital controllers to be implemented.

The effective implementation of an active control system relies on an understanding of both the electrical control issues involved (Elliott and Nelson, 1993) and the physics of either the acoustic or structural system being controlled (Nelson and Elliott, 1992; Fuller *et al.*, 1996).

In this review paper the physical limitations on the performance of an active sound or vibration control system are first illustrated by considering both the minimisation of total energy and the creation of a zone of quiet for the vibration on a plate and the sound inside an enclosure. This clearly shows that there is a frequency above which active control cannot generally be usefully applied, which depends on either the size of the whole system or the size of the zone of quiet compared with the wavelength of the disturbance.

The control issues are then introduced by considering two examples of the plant response in active control systems. The first system is for the control of vibration on a plate, and this shows clearly modal behaviour over a wide range of frequencies. The second system considered is the response between a secondary loudspeaker and a microphone in an acoustically well-damped enclosure such as a car interior. Although the response in this case can be described in terms of a modal summation, the separation between the modes is so small compared with the bandwidth that the frequency response does not have resonant peaks.

In many cases where active control can be used to control low frequency sound or vibration, the disturbance is originally generated by a rotating or a reciprocating ma-

chine. The measured disturbance is almost periodic for these cases, and its frequency can be readily measured using a tachometer on the machine, for example. Feedforward methods have been widely used for active control systems in such applications, with an external reference signal derived from the tachometer being used to drive the secondary sources via a controller which is adapted to minimise the disturbance measured at a number of error sensors (Elliott and Nelson, 1993). The algorithms used to adjust these adaptive feedforward controllers were developed from those used in numerical optimisation or adaptive signal processing, but will be analysed here in terms of an exactly equivalent feedback system. This illustrates the "closed loop" nature of adaptive feedforward control and also suggests how the tools of modern feedback control theory can be used to improve the performance and robustness of these algorithms. It also demonstrates how the stability of such adaptive controllers can be proved with relatively few, well defined, assumptions. For broadband disturbances propagating in a clearly defined direction, a reference signal can often be obtained from a detection sensor close to the primary noise source, which provides useful time-advanced information about the disturbance to be cancelled. Adaptive feedforward controllers have thus been extensively used for the active control of random sound propagating in ducts, for example (Eriksson *et al.*, 1987).

Finally, the active control of random disturbances will be discussed for the case in which no external reference signal is available and so a feedback control strategy must be used. It is difficult, for example, to obtain reliable reference signals if the disturbance is generated by numerous uncorrelated primary sources spatially distributed around the point at which control is required. An important example of such a case is the sound generated by the turbulent boundary layer in an aircraft, which is due to a very large number of eddies in the airstream outside the aircraft, each producing their own random contributions. Analogue feedback controllers have previously been used to control the sound inside active headsets and there is considerable interest at the moment in being able to extend such feedback methods to control random soundfields over larger regions of space. The aim of such a feedback control system is the rejection of the disturbances due to the primary sources, rather than tracking of a set point or desired signal. Feedback systems for the active control of sound and vibration are analysed here using the Internal Model Control architecture (Morari and Zafiriou, 1989). This allows the important trade-offs between performance and robustness to be explored and also provides a very convenient method of calculating the disturbance attenuation which can be optimally achieved with various delays in the plant. In practice, this will determine the maximum distance between the secondary source and the error sensor in an active control system and thus the physical size of the region which can be actively controlled.

2. Physical Limits to Active Control

In this section the physical limitations of two active control strategies will be illustrated for both the active control of vibration on a plate, and the active control of sound in an enclosure. Because we are interested in the ultimate physical limitations of these strategies, the electrical control problem will be made as simple as possible

by assuming that the disturbance is tonal and of known frequency, so that only the amplitude and phase of the secondary source(s) need be adjusted at any one frequency to minimise a physically motivated cost function.

2.1. Active Control of Vibrational Kinetic Energy on a Plate

The complex out-of-plane velocity at a point (x, y) on a plate can be expressed as a modal series, for steady state excitation at frequency ω as (Fuller *et al.*, 1996)

$$v(x, y, \omega) = \sum_{n=1}^{\infty} a_n(\omega)\phi_n(x, y) \tag{1}$$

where $a_n(\omega)$ is the complex amplitude and $\phi_n(x, y)$ is the corresponding mode shape of the n-th mode. The structural modes are assumed to be orthogonal and normalised so that

$$\frac{1}{S}\int_S \phi_n(x, y)\phi_m(x, y)\,\mathrm{d}x\,\mathrm{d}y = \begin{cases} 1 & \text{if} \quad n = m \\ 0 & \text{if} \quad n \neq m \end{cases} \tag{2}$$

where S is the surface area of the plate.

The total structural kinetic energy stored in the plate is given by the surface integral over the plate area of half the local mass multiplied by the mean square velocity, which for a uniform plate can be written as

$$E_k(\omega) = \frac{M}{4S}\int_S v^*(x, y, \omega)v(x, y, \omega)\,\mathrm{d}x\,\mathrm{d}y \tag{3}$$

where M is the total plate mass.

If the complex velocity is expressed in terms of the modal series (1), and using the orthonormal property of the modes, the total kinetic energy can also be expressed as

$$E_k(\omega) = \frac{M}{4}\sum_{n=1}^{\infty} |a_n(\omega)|^2 \tag{4}$$

i.e. is proportional to the sum of the modules squared mode amplitudes. To represent realistic physical systems, the summation can be truncated to a finite number of modes with arbitrarily small error. It is the total kinetic energy which is used here as a global measure of the response of the plate.

When the plate is excited by a primary force distribution and M secondary point forces, $f_{s1}, \ldots, f_{sM}$, then the complex amplitude of the n-th mode can be written as

$$a_n(\omega) = a_{np}(\omega) + \sum_{m=1}^{M} B_{nm} f_{sm} \tag{5}$$

where B_{nm} is the coupling coefficient between the m-th actuator and n-th mode, which is proportional to $\phi_n(x, y)$ at the point of application of the m-th secondary force.

Since a finite number of modes are assumed, eqn. (5) can be written in vector terms as

$$\boldsymbol{a} = \boldsymbol{a}_p + \boldsymbol{B}\boldsymbol{f}_s \tag{6}$$

where $a_{np}(\omega)$ is the amplitude of the n-th mode due to the primary force distribution and $\boldsymbol{B}$ is the matrix of coupling coefficients.

The total structural kinetic energy can now be written as

$$E_k = \frac{M}{4}\boldsymbol{a}^H\boldsymbol{a} = \frac{M}{4}\left[\boldsymbol{f}_s^H\boldsymbol{B}^H\boldsymbol{B}\boldsymbol{f}_s + \boldsymbol{f}_s^H\boldsymbol{B}^H\boldsymbol{a}_p + \boldsymbol{a}_p^H\boldsymbol{B}\boldsymbol{f}_s + \boldsymbol{a}_p^H\boldsymbol{a}_p\right] \tag{7}$$

where ^{H} denotes the Hermitian, complex conjugate, transpose. E_k is thus a Hermitian quadratic function of the real and imaginary parts of each of the secondary forces. This is guaranteed to have a global minimum, since the matrix $\boldsymbol{B}^H\boldsymbol{B}$ must be positive definite, which is obtained for a secondary force vector of

$$\boldsymbol{f}_s(\text{opt}) = -\left[\boldsymbol{B}^H\boldsymbol{B}\right]^{-1}\boldsymbol{B}^H\boldsymbol{a}_p \tag{8}$$

which results in a minimum value of kinetic energy given by

$$E_k(\text{min}) = \frac{M}{2}\boldsymbol{a}_P^H\left[\boldsymbol{I} - \boldsymbol{B}\left[\boldsymbol{B}^H\boldsymbol{B}\right]^{-1}\boldsymbol{B}^H\right]\boldsymbol{a}_p \tag{9}$$

Thus, given the primary force distribution, the properties and boundary conditions of the plate, from which the mode shapes can be calculated, and the positions of the secondary sources, the minimum possible total kinetic energy can be calculated after active control for each of a set of discrete excitation frequencies.

Figure 2 shows the physical arrangement for a computer simulation of active minimisation of total kinetic energy on a plate. The steel plate was assumed to have dimensions 380 mm × 300 mm × 1 mm thick, with an internal loss factor of 1% of critical damping and to be simply supported at the edges.

The total kinetic energy of the plate due only to the primary point force, f_p, positioned at $(x, y) = (270, 342)$ mm, is plotted for a range of discrete excitation frequencies as the solid line in Fig. 3. The dashed line shows the level of total kinetic energy after it has been minimised using a single secondary force, f_{s1}, at (30,38) mm and the dashed-dotted line shows the level after minimisation with this and two additional secondary forces, f_{s2} and f_{s3}, at (30,342) mm at (270,38) mm. These results have been obtained by minimising the total kinetic energy at a large number of individual discrete frequencies over the frequency range shown. This represents the limits of performance due only to the physical aspects of the active control problem, and the performance with a practical control system operating on a more complicated primary waveform will inevitably be worse than this. The positions of the primary and secondary sources close to the corners of the plate were chosen to enable them to couple into all the low order structural modes of the plate within this bandwidth. The single secondary force is clearly able to suppress the resonant response of individual modes of the plate below about 200 Hz. Above this frequency several modes with similar natural frequencies can be simultaneously excited by the primary source, when

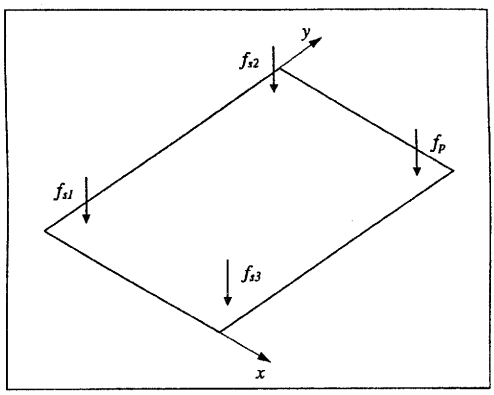

Fig. 2. Physical arrangement for active control of vibration on a plate by a primary point force, f_p, near one corner and either a single secondary point force, f_s, near the opposite corner.

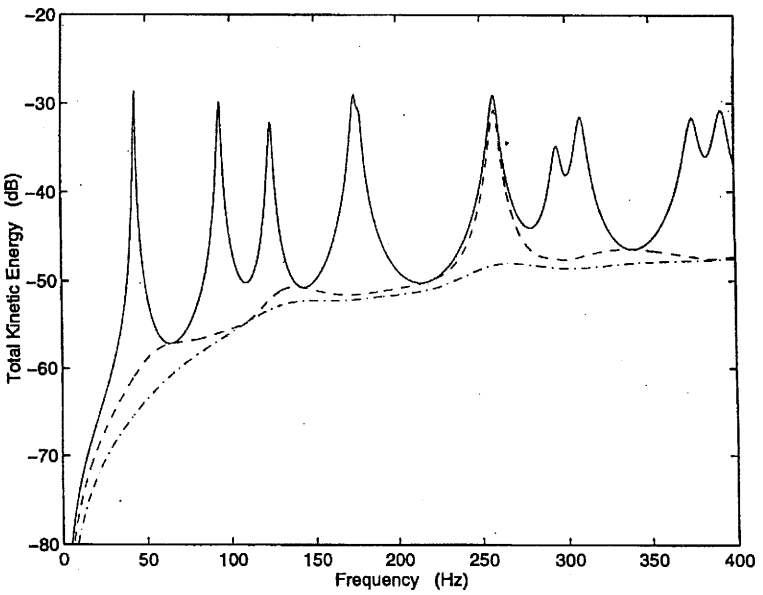

Fig. 3. Total kinetic energy of vibration on a plate when driven by the primary point force, f_p, alone at discrete frequencies (solid line) and after the total kinetic energy has been minimised by a single secondary force, f_{s1}, optimally adjusted at each excitation frequency (dashed line) or three secondary forces, f_{s1}, f_{s2} and f_{s3}, optimally adjusted at each excitation frequency (dash-dot line).

driven at 280 Hz for example, which cannot all be controlled by this single primary source. The use of three secondary forces solves this problem since the combination of secondary forces can independently couple into the two modes contributing to the primary response at 260 Hz and thus achieve control. Notice, however, that between the frequencies at which the resonant responses occur, relatively small reductions in energy can be achieved because of the large number of modes which contribute to the response at these frequencies.

2.2. Active Control of Total Acoustic Potential Energy in an Enclosure

The complex pressure in an enclosure due to an acoustic source distribution operating at a single frequency can be represented by a modal summation exactly analogous to eqn. (1) (Nelson and Elliott, 1992). The total acoustical potential energy in such an enclosure is proportional to the space average mean square pressure and can be written as

$$E_p(\omega) = \frac{1}{4\rho_0 c_0^2} \int_V \left| p(x, y, z, \omega) \right|^2 \mathrm{d}V \tag{10}$$

where ρ_0 and c_0 are the density and speed of sound in the medium, $p(x, y, z, \omega)$ is the complex acoustic pressure at the point (x, y, z) and at the frequency ω in the enclosure and V is the total volume of the enclosure. The total acoustic potential energy provides a convenient cost function for evaluating the effect of global active control of sound in an enclosure.

Because of the assumed orthonormality of the acoustic modes, E_p can again be shown to be proportional to the sum of the squared mode amplitudes, and these mode amplitudes can again be expressed in terms of the contribution from the primary and secondary sources, as in eqn. (6). Thus the total acoustic potential energy is a Hermitian quadratic function of the complex strengths of the secondary acoustic sources, which can be minimised in exactly the same way as described above.

A simulation has been carried out of minimising the total acoustic potential energy in an enclosure of dimensions $1.9 \times 1.1 \times 1.0$ m as illustrated in Fig. 4, in which the acoustic modes have an assumed damping ratio of 10% of critical, which is fairly typical for a reasonably well damped acoustic enclosure such as a car interior at low frequencies. Figure 5 shows the total acoustic potential energy in the enclosure when driven by only the primary source placed in one corner of the enclosure and when the total acoustic potential energy is minimised by a single secondary acoustic source in the opposite corner (dashed line) or by seven secondary acoustic sources positioned at each of the corners of the enclosure not occupied by the primary source (dash-dot line). The positions of the secondary sources were chosen to allow them to couple into the acoustic modes within the enclosure (Nelson and Elliott, 1992). Better active control performance could be obtained if a secondary source was positioned very close to the primary source, but only because of the unrealistic assumption that the primary source only acts at a point in this example.

In this case the response of the system does not show clear modal behaviour for excitation frequencies above about 150 Hz, and very little attenuation can be achieved

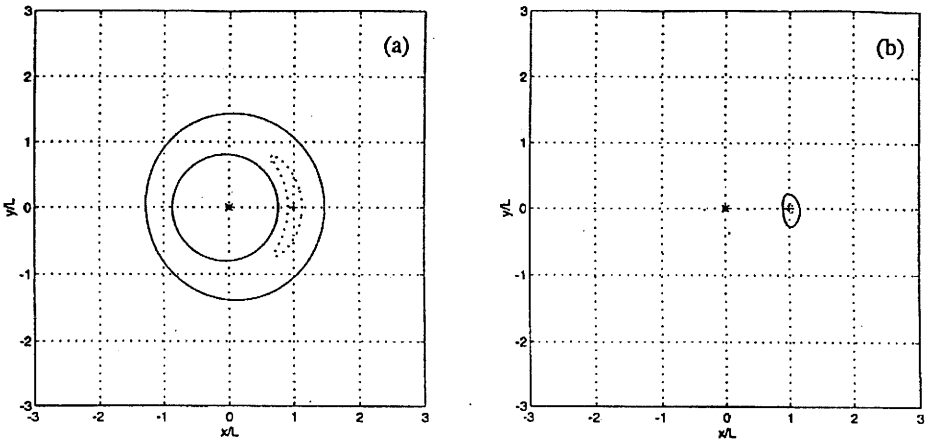

Fig. 8. The spatial extent of the acoustic "zone of quiet" generated by cancelling the pressure at $x/L = 1$ in a three dimensional free field using a point monopole acoustic secondary source at the origin of the co-ordinate system for (a) $L = 0.03\lambda$ and (b) $L = 0.3\lambda$ where λ is the acoustic wavelength. The solid line corresponds to a 10 dB attenuation in the diffuse primary field, and the dashed line to a 20 dB attenuation.

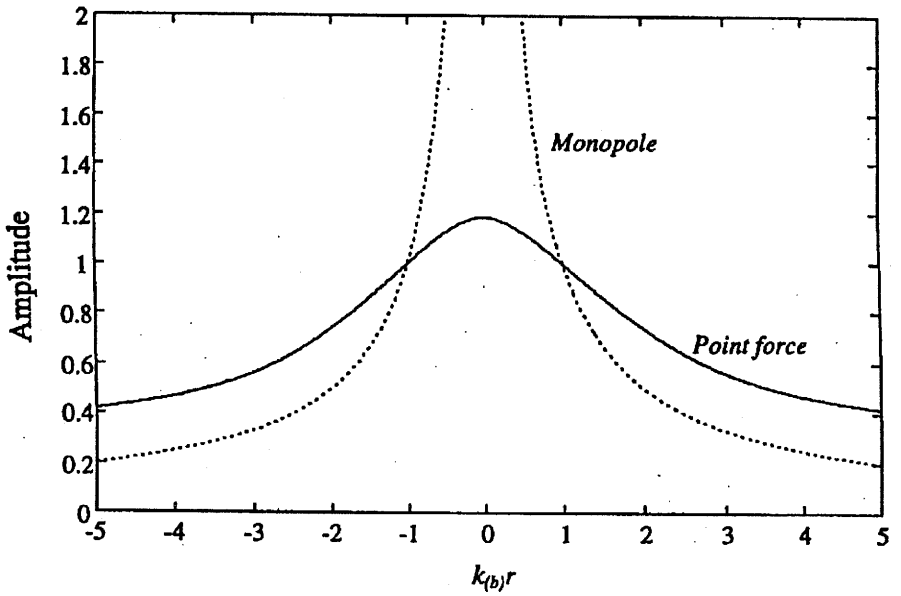

Fig. 9. The near-field velocity due to a point force acting on an infinite plate (solid line) and the near-field pressure due to an acoustic monopole source in free space (dashed line).

a "shell" of cancellation. At higher frequencies in the acoustic case, when $L \geq \lambda/10$, then the zone of quiet does not form a complete shell but is concentrated in a sphere centred on the cancellation point, whose diameter is about $\lambda/10$ (Elliott *et al.*, 1988a; 1988b).

The advantage of a local control system is that the secondary source does not have to drive very hard to achieve control, because it is very well coupled to the response at the cancellation point. Local zones of quiet can often thus be generated without significantly affecting the overall energy in the system.

At low frequencies, where the wavelength of the disturbance is comparable to the dimensions of the system under control, then global active control is feasible, and at higher frequencies it is still possible to achieve local active control over a region of the system which is small compared to the wavelength of the disturbance.

3. Plant Response

In order to allow active control systems to be easily adapted, they are often implemented "digitally", i.e. as a sampled data system. Because the frequencies being controlled are relatively low in audio terms, as explained above, any distortion generated by the digital to analogue converters would occur in a frequency region in which the ear is particularly sensitive and so this is generally avoided by the use of analogue reconstruction filters. Similarly, analogue anti-aliasing filters are generally used to remove disturbances above half the sample rate before digital to analogue conversion, which would otherwise cause audible distortion. If driven by an analogue pure tone, the digital controller and data filters in this case thus only produce an analogue pure tone response and so act linearly with respect to the outside world. Hence the full theory of sample data-systems, with a transformation from the s domain to the z domain which includes aliased components (Franklin *et al.*, 1990), does not need to be used in this case, since aliasing is specifically prevented, and the sampled version of the sensor signals can be taken as a reasonably complete representation of these signals within the bandwidth of the controller. The disadvantage of using these anti-aliasing and reconstruction filters is their significant group delay, which contributes to the overall delay in the plant and can become comparable with the physical delays in the system under control.

The plant response in a digital active control system is assumed to include all of these analogue filters, together with the dynamic response of the secondary actuator and disturbance sensor, and the structural or acoustic response of the physical system under control. The measured plant responses from two examples of active control systems are presented here to illustrate the typical differences between a structural and an acoustic response.

Figure 10 shows the measured frequency response and impulse response of an aluminium plate excited by a small piezoceramic (PZT) actuator bonded to one side of the plate and measured using a distributed piezoelectric (PVDF) film sensor, designed to measure the net volume displacement of the plate (Johnson and Elliott, 1995). In this example of a structural response the response of individual modes can be clearly

seen over the whole frequency range, because the modal overlap is relatively low in this case, as discussed in Section 2. The impulse response has a strong reverberant component and continues at a significant level for about 90 ms.

For many control algorithms the plant response must be internally modelled by the controller. For the structural response shown in Fig. 10 a recursive (IIR) model is clearly appropriate and it was found that when sampled at 2 kHz an acceptable model could be designed with 24 direct and 24 recursive coefficients, whereas 180 coefficients would be required for an FIR filter of comparable accuracy.

Figure 11 shows the frequency responses and impulse response measured from a loudspeaker, acting as a secondary actuator, to a pressure microphone, acting as a disturbance sensor, inside the passenger cabin of a car. In contrast to the structural case, there is almost no modally resonant component in this frequency response. The acoustic enclosure is very heavily damped in this case and the most noticeable features are the zeros in the frequency response, caused by interference between the various acoustic modes at the location of the microphone. The impulse response shows a delay of about 5 ms which is partly due to acoustic propagation time and partly due to delays in the analogue data conversion filters. Most noticeable, however, is the short duration of the impulse response compared with the structural case. The impulse response in Fig. 11(c) is concentrated in a region from about 5 ms to 30 ms. The sampling frequency of the control system in this case was 1 kHz and an accurate model of the plant could be obtained with only 25 coefficients by directly modelling the impulse response with an FIR filter. Such a filter is unconditionally stable and it is very easy to directly adapt its coefficients, which makes it well suited to rapid system identification (Widrow and Stearns, 1985).

4. Adaptive Feedforward Control

Adaptive feedforward methods are very widely used in active control to reject periodic disturbances of known frequency. The algorithms which are used in these adaptive systems generally have their origins in either the signal processing literature (Widrow and Stearns, 1985) or the numerical optimisation literature (Press *et al.*, 1986), and operate in either the time domain or the frequency domain. Some of these algorithms will be described in this section, together with an interpretation of their behaviour in terms of an equivalent feedback controller.

4.1. Frequency Domain Algorithms

We begin with the simple case of a single channel, SISO, controller adapted in the frequency domain using the steepest descent algorithm to reject a tonal disturbance. The block diagram of such a system is shown in Fig. 12 and we will initially assume that the disturbance, $d(j\omega_0)$, is stationary and any transients in the plant caused by a prior change have died away, so the plant is operating in its steady state and can be characterised by its complex response at the excitation frequency ω_0 only, which is $G(j\omega_0)$. The complex error signal under these conditions is thus given by

$$e(j\omega_0, n) = d(j\omega_0) + G(j\omega_0)u(j\omega_0, n) \tag{13}$$

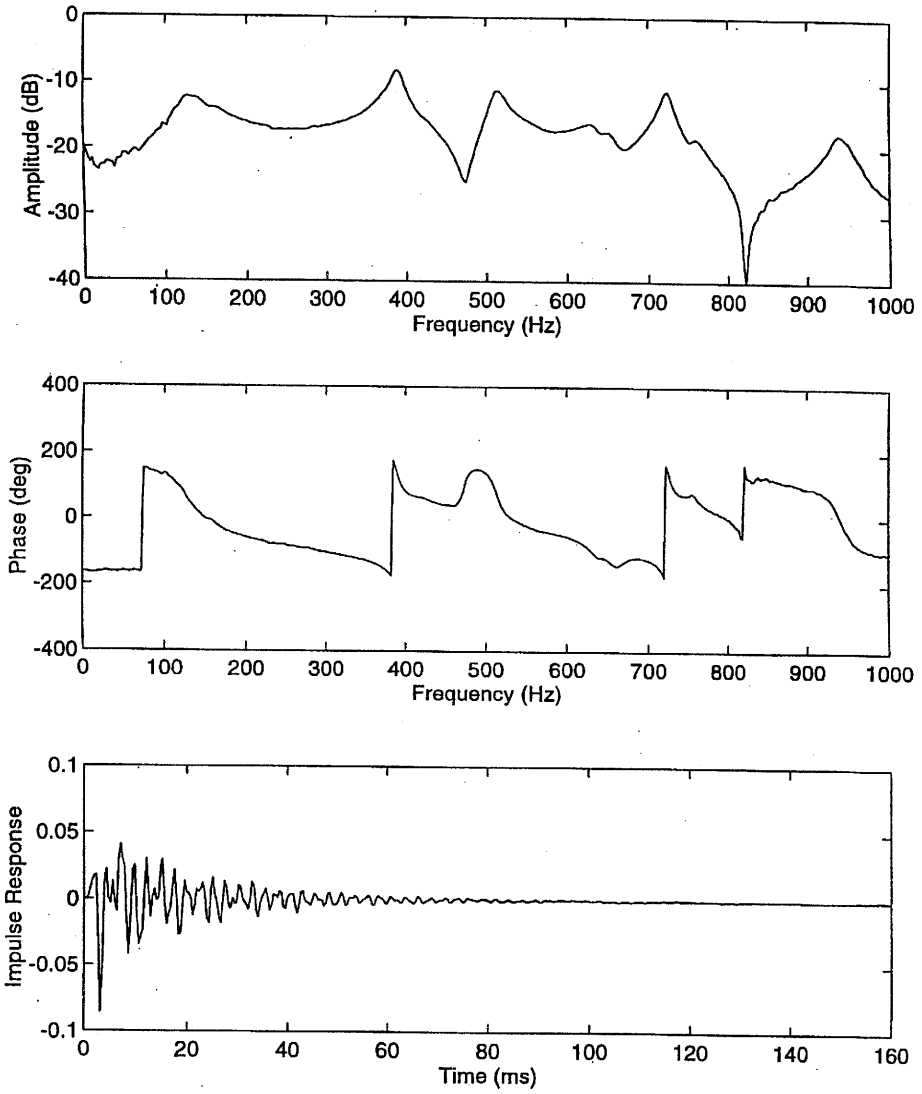

Fig. 10. The modulus and phase of the frequency response of an aluminium plate excited by a piezoceramic actuator and measured using a distributed piezoelectric film sensor. The impulse response of the system is also shown.

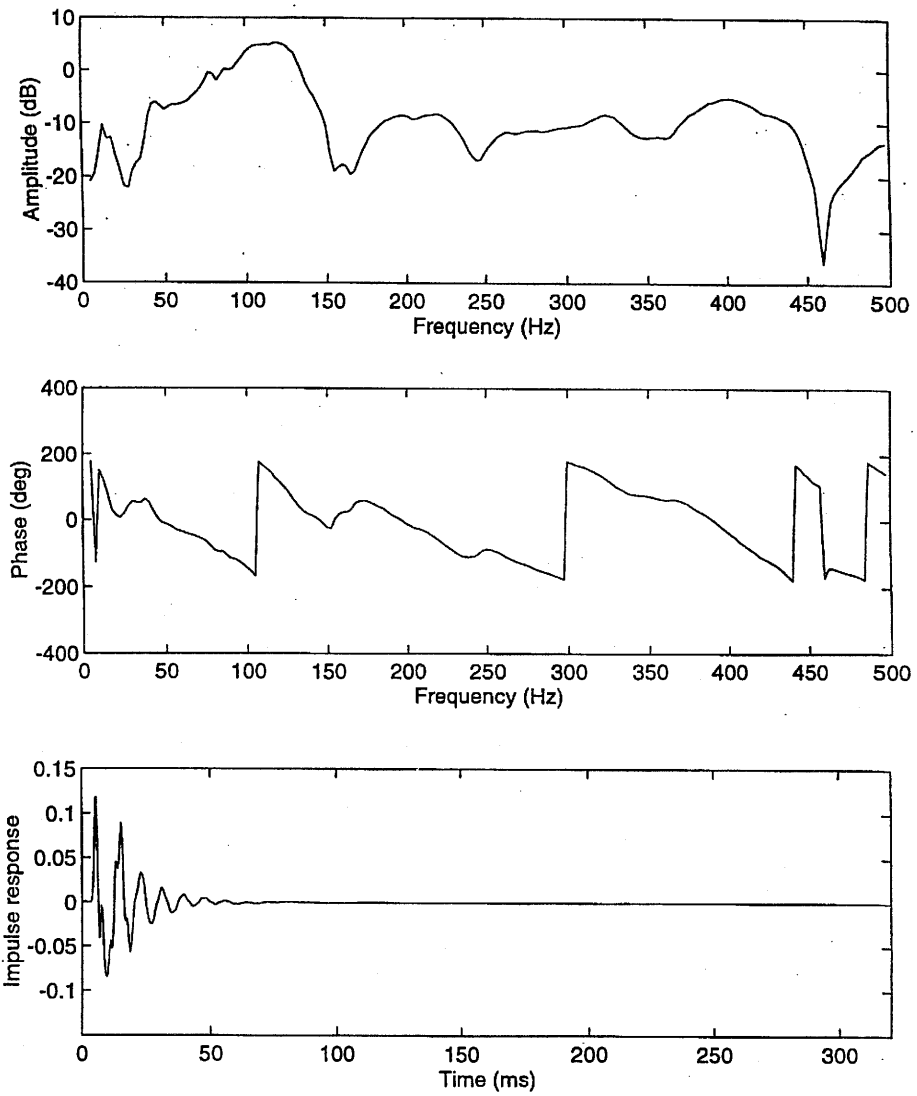

Fig. 11. The modulus and phase of the frequency response of an acoustic enclosure excited by a loudspeaker and measured using a pressure microphone. The impulse response of the system is also shown.

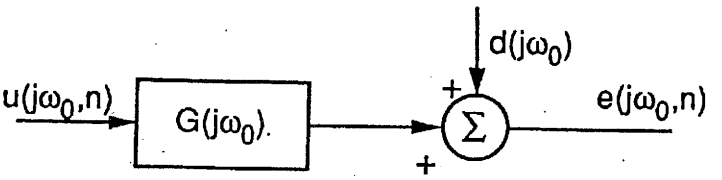

Fig. 12. Block diagram of a single channel feedforward control system operating at a single frequency, ω_0.

where $u(j\omega_0, n)$ is the complex input to the plant from the controller at the n-th iteration of the controller.

The modulus squared error is a quadratic function of the real and imaginary parts of $u(j\omega_0, n)$ with a unique global minimum. The complex gradient of this quadratic function can be defined to be (Elliott and Nelson, 1993)

$$\frac{\partial |e(j\omega_0, n)|^2}{\partial \operatorname{Re}\left(u(j\omega_0, n)\right)} + j\frac{\partial |e(j\omega_0, n)|^2}{\partial \operatorname{Im}\left(u(j\omega_0, n)\right)} = 2G^*(j\omega_0)e(j\omega_0, n) \tag{14}$$

where the (real) derivatives with respect to the real and imaginary parts have been gathered together into a single complex number for convenience and * denotes conjugation. Note that we are not using a derivative with respect to a complex number and so the problems associated with the cost function not being analytic (see e.g. Haykin, 1996, Appendix B) are avoided. If the real and imaginary parts of $u(j\omega_0, n)$ are now adjusted using the method of steepest descents then using (14) the update algorithm can be written as

$$u(j\omega_0, n+1) = u(j\omega_0, n) - \alpha \hat{G}^*(j\omega_0)e(j\omega_0, n) \tag{15}$$

where α is a (real) adaptation coefficient, and $\hat{G}(j\omega_0$ is an estimate of the complex plant response used by the adaptive algorithm.

It could be argued that if the error is given by eqn. (13), and the plant estimate $\hat{G}(j\omega_0)$ was perfectly accurate, then $e(j\omega_0, n+1)$ could be set to zero in one iteration by using the algorithm

$$u(j\omega_0, n+1) = u(j\omega_0, n) - \hat{G}^{-1}(j\omega_0)e(j\omega_0, n) \tag{16}$$

Notice, however, that the phase of $\hat{G}^{-1}(j\omega_0)$ is the same as that of $\hat{G}^*(j\omega_0)$ and if $a = (|\hat{G}(j\omega_0)|^2)^{-1}$ in eqn. (15), it is identical to eqn. (16). In the SISO case the iterative exact least squares solution is thus obtained as a special case of the steepest descent algorithm, with a particular value of convergence coefficient.

We now consider the sequence of complex steady state values of $u(j\omega_0, n)$ and $e(j\omega_0, n)$ as a sampled time history, with z transforms $u(z)$ and $e(z)$, and take the z transform of eqn. (15), to give

$$u(z) = \frac{-\alpha}{z-1}\hat{G}^*(j\omega_0)e(z) \tag{17}$$

The adaptive feedforward controller in this case can be interpreted as a fixed feedback controller, sampled at a slow enough rate for the plant transients to die away between sample times. Taking the z transform of eqn. (10), we obtain

$$e(z) = d + Gu(z) \tag{18}$$

The equivalent block diagram for this interpretation of the adaptive feedforward controller is thus of the form shown in Fig. 13, where G is now just a complex gain, and the negative "feedback controller" has the transfer function

$$H(z) = \frac{\alpha}{z-1}\hat{G}^*(j\omega_0) \tag{19}$$

The term $\lambda/(z-1)$ is a digital integrator and so, provided the system is stable, the control loop will exactly compensate for any observed error over a timescale determined by the 'gain' parameter λ.

The function of the term $\hat{G}^*(j\omega_0)$ in eqn. (19) is to compensate for the phase of the plant at the excitation frequency, so that ideally, if $\hat{G}(j\omega_0) = G(j\omega_0)$, the real and imaginary parts of $e(n)$ respond independently. The feedback controller shown in Fig. 13 has a single pole given by

$$z = 1 - \alpha G(j\omega_0)\hat{G}^*(j\omega_0) \tag{20}$$

and will thus be stable providing α is small and positive and the real part of $G(j\omega_0)\hat{G}^*(j\omega_0)$ is positive, which is ensured providing that the phase of $\hat{G}(j\omega_0)$ is within $\pm 90°$ of that of $G(j\omega_0)$, (Elliott *et al.*, 1987; Morgan, 1980).

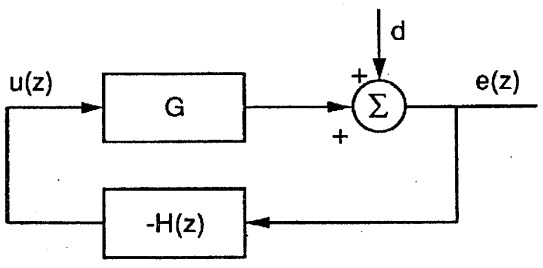

Fig. 13. Equivalent feedback system for the iteratively adapted frequency-domain feedforward algorithm.

Multichannel (MIMO) frequency domain adaptive feedforward control systems can be treated in an exactly analogous way. In this case the vector of complex steady-state error signals at the n-th iteration is given by

$$\boldsymbol{e}(j\omega_0, n) = \boldsymbol{d}(j\omega_0) + \boldsymbol{G}(j\omega_0)\boldsymbol{u}(j\omega_0, n) \tag{21}$$

where $\boldsymbol{G}(j\omega_0)$ is now the matrix of complex responses between each secondary actuator and each error sensor at the excitation frequency. Similarly, the adaptive steepest descent algorithm becomes

$$\boldsymbol{u}(j\omega_0, n+1) = \boldsymbol{u}(j\omega_0, n) - \alpha\hat{\boldsymbol{G}}^H(j\omega_0)\boldsymbol{e}(j\omega_0, n) \tag{22}$$

Taking the z transform of eqn. (22) leads to the equivalent MIMO feedback controller in this case, so that in the z domain the vector of error signals becomes

$$\boldsymbol{e}(z) = \left[\boldsymbol{I} + \boldsymbol{G}\boldsymbol{H}(z)\right]^{-1}\boldsymbol{d}(z) \tag{23}$$

where in this case $\boldsymbol{G}$ is equal to $\boldsymbol{G}(j\omega_0)$ and

$$\boldsymbol{H}(z) = \frac{\alpha}{z-1}\hat{\boldsymbol{G}}^H(j\omega_0) \tag{24}$$

The stability of the MIMO system is governed by the poles of the system. These are the roots of the characteristic equation obtained by setting the determinant of the equation

$$\boldsymbol{I} + \boldsymbol{G}\boldsymbol{H}(z) = \boldsymbol{I} + \frac{\alpha}{z-1}\boldsymbol{G}(j\omega_0)\hat{\boldsymbol{G}}^H(j\omega_0) \tag{25}$$

to zero. The pole positions are thus given by

$$z_i = 1 - \alpha\lambda_i \tag{26}$$

where λ_i is the i-th eigenvalue of $\boldsymbol{G}(j\omega_0)\hat{\boldsymbol{G}}^H(j\omega_0)$. The MIMO system will thus be stable provided $|z_i| < 1$ for all λ_i, which is equivalent to the condition

$$0 < \alpha < \frac{2\,\mathrm{Re}\,(\lambda_i)}{|\lambda_i|^2} \qquad \text{for all} \quad \lambda_i \tag{27}$$

For slow convergence, small α, eqn. (27) implies that for stability the real parts of each of the eigenvalues of $\boldsymbol{G}(j\omega_0)\hat{\boldsymbol{G}}^H(j\omega_0)$ must be positive. This condition has previously been derived (Elliott *et al.*, 1992) from an analysis of the iterative convergence of eqn. (22).

Assuming the plant model is perfect, the iterative algorithm is guaranteed to be stable, for small α, since the eigenvalues of the Hermitian matrix $\boldsymbol{G}(j\omega_0)\,\boldsymbol{G}^H(j\omega_0)$ are either positive or zero. Under these conditions the convergence of the control system can be decomposed into a set of "modes" which each converge independently with a time constant proportional to $1/\lambda_i$ (Elliott *et al.*, 1992). The non-zero eigenvalues of the matrix $\boldsymbol{G}(j\omega_0)\,\boldsymbol{G}^H(j\omega_0)$ calculated from a measured matrix of transfer responses are shown in Fig. 14 (Elliott *et al.*, 1992). The transfer response matrix

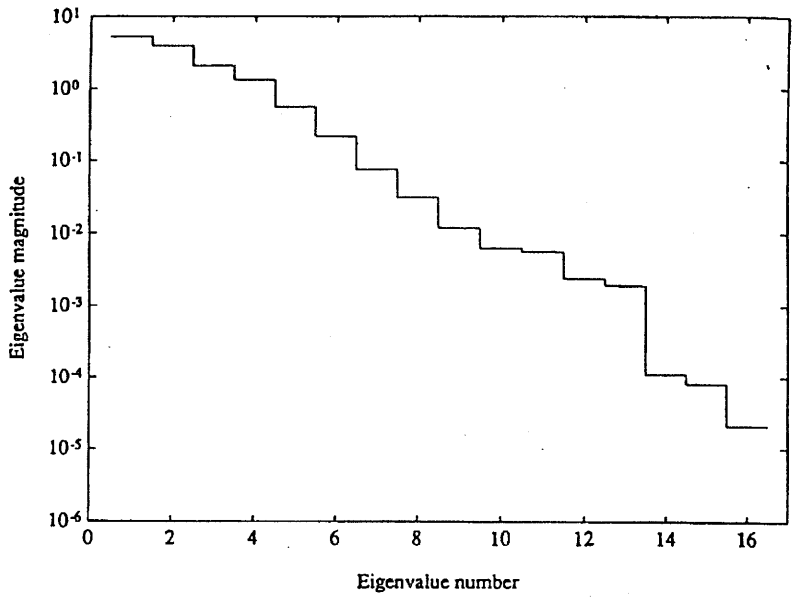

Fig. 14. The eigenvalues of the matrix $\boldsymbol{G}(j\omega_0)\,\boldsymbol{G}^H(j\omega_0)$ for the acoustic transfer response measured from 16 loudspeakers to 32 microphones in an enclosure excited at 88 Hz.

$\boldsymbol{G}(j\omega_0)$ was measured from 16 loudspeakers to 32 microphones in a 6 m × 2.2 m × 2.2 m enclosure at an excitation frequency of 88 Hz. The eigenvalues are entirely real in this case and have a range of about 10^6. The large range of eigenvalues suggests that in this case the system is very ill-conditioned. This is because a larger number of loudspeakers have been used to control the soundfield at this excitation frequency than were necessary from an analysis of the number of acoustic modes being excited. This is a not-uncommon situation in active control, however, where the number of actuators may be chosen to ensure good control under worst-case conditions, e.g. higher frequency excitation, but the system often has to operate under conditions in which the number of actuators is over specified.

An example of the convergence of the sum of the squared errors at the 32 microphones is shown in Fig. 15 for an adaptive feedforward active sound control system operating in this enclosure. Several control modes with large eigenvalues are significantly excited by the primary disturbance and these decay away relatively quickly to give an attenuation of 20 dB in the sum of squared errors. The modes with the smaller eigenvalues die away more slowly, and the sum of squared errors is eventually reduced by more than 30 dB. In practice, however, it is the rapid initial convergence which has the largest subjective effect.

In practice the plant model is not perfect and for systems with large numbers of actuators and sensors it is likely that some of the eigenvalues of $\boldsymbol{G}(j\omega_0)\,\hat{\boldsymbol{G}}^H(j\omega_0)$ will have small negative real parts, which gives rise to slow unstable modes. One method of

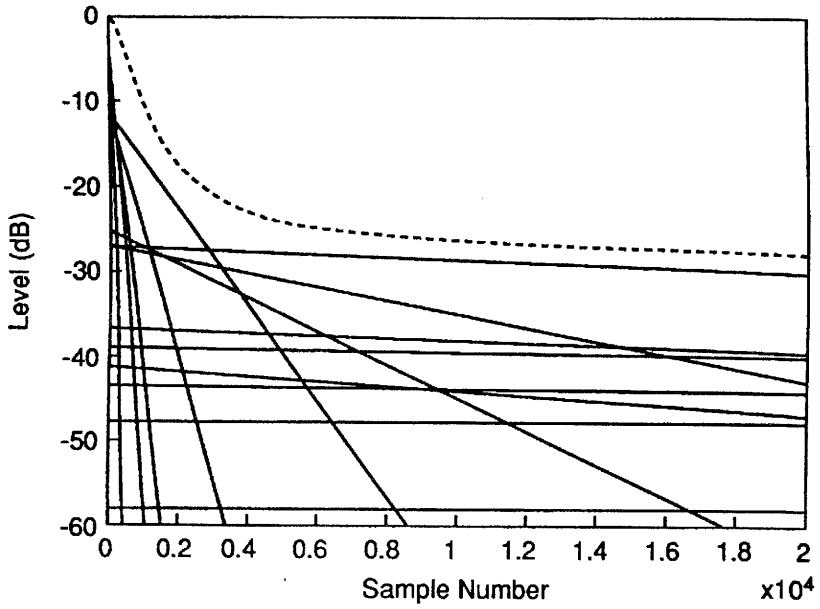

Fig. 15. The level of the reduction in the sum of squared errors against time for the overall convergence of an iterative multichannel feedforward controller controlling the sum of squared errors at 32 microphones with 16 loudspeakers (dashed curve). Also shown is the convergence behaviour of the individual 'modes' of the control system (solid lines).

making the control system more robust to such uncertainty is to implement a steepest descent algorithm which minimises the sum of squared errors and a real parameter, β, times the sum of squared control efforts. Equation (22) then becomes (Elliott *et al.*, 1992)

$$\boldsymbol{u}(j\omega_0, n+1) = (1-\alpha\beta)\boldsymbol{u}(j\omega_0, n) - \alpha\hat{\boldsymbol{G}}^H(j\omega_0)\boldsymbol{e}(j\omega_0, n) \tag{28}$$

which is referred to as a 'leaky' algorithm in the signal processing literature (Widrow and Stearns, 1985). The equivalent feedback controller in this case is equal to

$$\boldsymbol{H}(z) = \frac{\alpha}{z-1+\alpha\beta}\hat{\boldsymbol{G}}^H(j\omega_0) \tag{29}$$

and the perfect digital integrator in eqn. (24) has been replaced by a 'leaky' integrator. The stability of this control system is now determined by the eigenvalues of the matrix $[\boldsymbol{G}(j\omega_0)\hat{\boldsymbol{G}}^H(j\omega_0) + \beta\boldsymbol{I}]$ so that any eigenvalue of $\boldsymbol{G}(j\omega_0)\hat{\boldsymbol{G}}^H(j\omega_0)$ with a small negative real part can be compensated for by an appropriate positive value of β. Even if the plant model is perfect, the effort weighting parameter has the effect of reducing the range of eigenvalues in the control problem, thus reducing any ill-conditioning.

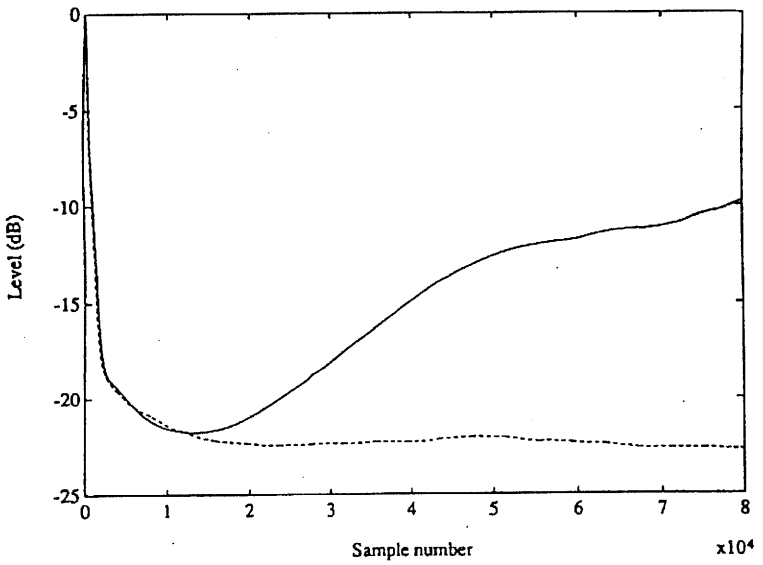

Fig. 16. The level of the sum of squared error signals when an adaptive feedforward control system with errors in the estimated plant response matrix is used to control the tonal disturbance at 32 microphones using 16 loudspeakers with no effort weighting in the cost function (solid line) and when a sufficient effort weighting (β) is included in the cost function to stabilise the system (dashed line).

The convergence behaviour of the multichannel controller described above when rather large random errors were introduced into the matrix $\hat{\boldsymbol{G}}(j\omega_0)$ is shown in Fig. 16 (Elliott *et al.*, 1992). The solid line shows the behaviour with the effort weighting parameter, β, equal to zero, in which case some of the control modes have small negative eigenvalues and are unstable. The unstable behaviour is only evident after the fast initial convergence, however, since the modes associated with the large eigenvalues are relatively unaffected. The exponential increase in the sum of squared errors is limited in practice by saturation of the loudspeaker amplifiers. If a suitable value of effort weighting parameter is included in the adaptive algorithm, the real parts of all the eigenvalues of the $[\boldsymbol{G}(j\omega_0)\hat{\boldsymbol{G}}^H(j\omega_0) + \beta\boldsymbol{I}]$ matrix will be positive and the control system is stabilised, as shown by the dashed line in Fig. 16. This level of β does not significantly affect the larger eigenvalues and thus the initial rapid convergence behaviour is largely unaffected.

If the slow modes of convergence in the steepest descent algorithm are a problem, algorithms based on Gauss-Newton methods could be used. This leads to an iterative algorithm of exactly the same form as eqn. (22) with the pseudo-inverse of the estimated plant response replacing its Hermitian transpose. Assuming there are more error sensors (L) than secondary sources (M), so that the problem is overdetermined, this pseudo-inverse is equal to

$$\hat{\boldsymbol{G}}^{\dagger}(j\omega_0) = \left[\hat{\boldsymbol{G}}^H(j\omega_0)\hat{\boldsymbol{G}}(j\omega_0)\right]^{-1}\hat{\boldsymbol{G}}^H(j\omega_0) \tag{30}$$

The transfer function matrix of the plant can be decomposed using the singular value decomposition, so that

$$\boldsymbol{G}(j\omega_0) = \boldsymbol{R}\,\boldsymbol{\Sigma}\,\boldsymbol{Q}^H \tag{31}$$

where $\boldsymbol{\Sigma}$ is the square diagonal matrix of singular values, or "principle gains" of the plant response at ω_0 (Maciejowski, 1989).

The Hermitian transpose of the plant response matrix is thus

$$\boldsymbol{G}^H(j\omega_0) = \boldsymbol{Q}\,\boldsymbol{\Sigma}\,\boldsymbol{R}^H \tag{32}$$

and the pseudo-inverse of $\boldsymbol{G}(j\omega_0)$ is equal to

$$\boldsymbol{G}^\dagger(j\omega_0) = \boldsymbol{Q}\,\boldsymbol{\Sigma}^{-1}\boldsymbol{R}^H \tag{33}$$

Assuming a perfect plant model, the convergence rates of modes of the steepest descent method have been shown to depend on the eigenvalues of the matrix

$$\boldsymbol{G}(j\omega_0)\boldsymbol{G}^H(j\omega_0) = \boldsymbol{R}\,\boldsymbol{\Sigma}^2\boldsymbol{R}^H \tag{34}$$

which are thus equal to the squared values of the principle gains. The convergence rates of the Gauss-Newton algorithm, however, will depend on the eigenvalues of the matrix

$$\boldsymbol{G}(j\omega_0)\boldsymbol{G}^\dagger(j\omega_0) = \boldsymbol{R}\,\boldsymbol{R}^H \tag{35}$$

which are either unity or zero. Thus the Gauss-Newton algorithm will, in principle, have modes of convergence with equal time constants.

The problem with the Gauss-Newton method is that there can be a number of the very small singular values, as seen in Fig. 14, which are subject to large uncertainties due to measurement errors or changes in the plant. The effect of these uncertainties is enormously amplified by the inversion of the singular values in eqn. (33) and can easily result in rapid instability if the plant model is not exactly equal to the true plant response. One solution to this robustness problem is to divide the singular values into two classes, based e.g. on the number required to achieve acceptable attenuations in the disturbance. A modified inverse matrix is then generated for use in eqn. (33) in which the larger singular values can be inverted, and the others are not. The modes of convergence associated with the well-conditioned singular values will thus all converge at the same, rapid, rate but the modes associated with the smaller uncertain values will be prevented from becoming unstable and may have small positive constants added for stabilisation.

4.2. Time Domain Algorithms

One of the most widely used adaptive algorithms used in active control is a variant of the 'LMS algorithm' introduced for the adaptation of digital filters by Widrow and Hoff (1960). This algorithm operates in the sampled time domain and the plant behaviour must now be represented by its full dynamic response, represented here by the set of impulse response operators, characterised by $g_{lm}(q)$, which is the one from

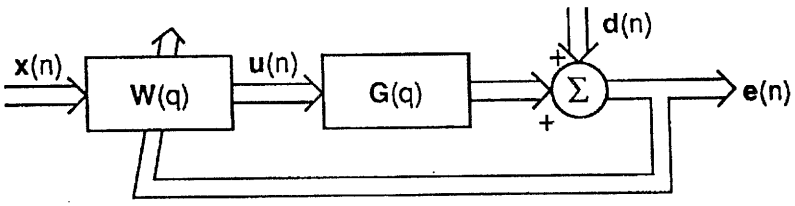

Fig. 17. Block diagram of a multichannel adaptive feedforward control system.

the m-th secondary actuator to the l-th error sensor. The time history of the l-th error sensor is thus given by

$$e_l(n) = d_l(n) + \sum_{m=1}^{M} g_{lm}(q)u_m(n) \tag{36}$$

where $u_m(n)$ is the signal driving the m-th secondary actuator. These signals are obtained by filtering a set of K reference signals, $x_k(n)$, by a matrix of control filters with finite impulse response operators $w_{mk}(q)$, as shown in Fig. 17, so that

$$u_m(n) = \sum_{k=1}^{K} w_{mk}(q)x_k(n) \tag{37}$$

The l-th error sequence can thus be written as

$$e_l(n) = d_l(n) + \sum_{m=1}^{M}\sum_{k=1}^{K} g_{lm}(q)w_{mk}(q)x_k(n) \tag{38}$$

or in a simpler form as

$$e_l(n) = d_l(n) + \sum_{m=1}^{M}\sum_{k=1}^{K} w_{mk}(q)r_{lmk}(n) \tag{39}$$

where the set of filtered reference signals is defined to be

$$r_{lmk}(n) = g_{lm}(q)x_k(n) \tag{40}$$

Notice that in reversing the order of the filtering in eqn. (38) we are implicitly assuming that both $g_{lm}(q)$ and $w_{mk}(q)$ are time-invariant at this stage. Equation (39) can now be written in matrix form as

$$\boldsymbol{e}(n) = \boldsymbol{d}(n) + \boldsymbol{R}(n)\boldsymbol{w} \tag{41}$$

where $\boldsymbol{R}(n)$ is a matrix of filtered reference signals and $\boldsymbol{w}$ is a vector of control filter coefficients. If these filter coefficients are adapted at every sample time to minimise the sum of the squared errors using an instantaneous estimate of the local derivative

of the error surface, then the adaptive algorithm can be written as (Elliott *et al.*, 1987),

$$\boldsymbol{w}(n+1) = \boldsymbol{w}(n) - \alpha \hat{\boldsymbol{R}}^T(n)\boldsymbol{e}(n) \tag{42}$$

where $\hat{\boldsymbol{R}}^T(n)$ is the filtered reference signals used in practice which are obtained from estimated plant responses. This algorithm is a multichannel generalisation of the filtered reference version of the LMS algorithm (Widrow and Stearns, 1985) and is known as the Multiple Error LMS algorithm. It has been widely used in systems actively to control propeller noise in aircraft (Elliott *et al.*, 1990) and engine noise in cars (Elliott *et al.*, 1988).

Figure 18, for example, shows the pressure distribution at 32 microphone positions in the passenger cabin of a propeller aircraft at the blade-passing frequency, 88 Hz, measured during a flight trial before and after control with an adaptive control system using 16 loudspeakers. Reductions of 14 dB in the sum of the squared microphone signals were measured at this frequency, and similar levels of reduction would be very difficult to obtain using passive control methods without a very significant weight penalty.

In the special case where the reference signal is a synchronously sampled sinusoid, the behaviour of the Multiple Error LMS algorithm can be shown to be *exactly* equivalent to the fixed multichannel feedback controller in which the feedback path from the l-th error signal to the m-th secondary actuator is given by (Elliott *et al.*, 1987)

$$H_{ml}(z) = \left[\frac{\alpha I}{2(1 - 2z\cos\omega_0 + z^2)}\right][A_{lm}z\cos(\omega_0 - \phi_{lm}) - \cos\phi_{lm}] \tag{43}$$

where ω_0 is the frequency of the reference signal and the complex plant response from the m-th secondary actuator to the l-th error sensor at this frequency is modelled as

$$\hat{G}_{lm}(j\omega_0) = A_{lm}e^{j\phi_{lm}} \tag{44}$$

The first term in the expression for $H_{ml}(z)$ can be recognised as an oscillator, whose amplitude will rise if the average value of the remaining part of eqn. (43) multiplied by the error signal is positive and fall if this driving term is negative. Whatever the value of the error signal, the equivalent feedback controller thus drives the plant with a time-varying sinusoid, as expected from eqn. (37). In the case of slow adaptation, small α, only the response at $z = e^{j\omega_0}$ is significant and the second term in the expression for $H_{ml}(z)$ in eqn. (43) becomes proportional to $\hat{G}^*_{lm}(e^{j\omega_0})$. The feedback controller in this case thus reduces to that for the iterative frequency domain controller. In general, however, the complete behaviour of the adaptive time domain controller in this case can be described by coupling the feedback controller given by eqn. (43) to the full dynamics of the plant in a negative feedback arrangement (see e.g. Elliott *et al.*, 1987; Morgan and Sanford, 1992; Sievers and von Flotow, 1992).

Of particular interest is the effect of plant delay on the bandwidth of the equivalent feedback controller. The plant delay limits the maximum value of the convergence

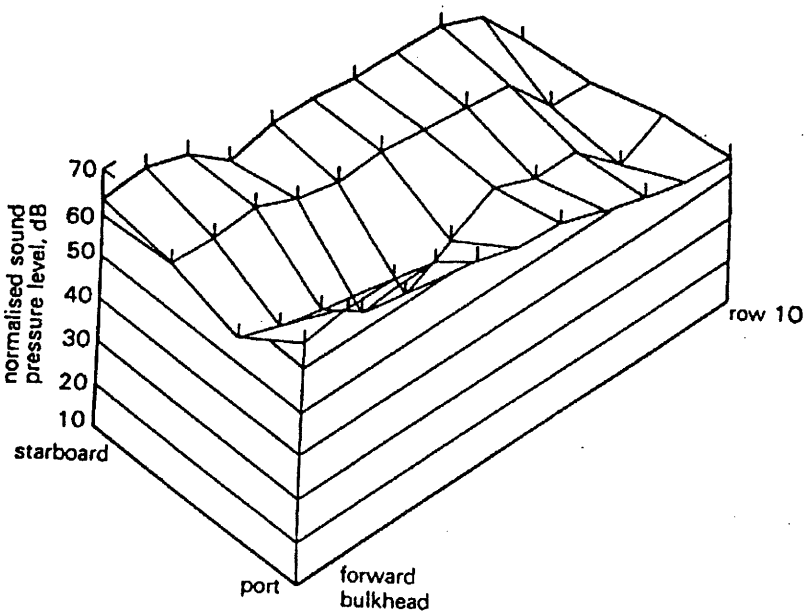

a)

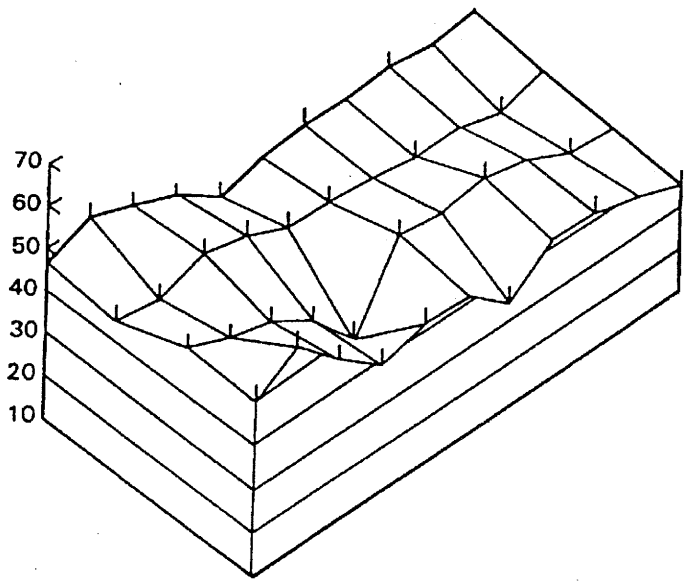

b)

Fig. 18. Spatial distribution of the normalised sound pressure level at 88 Hz measured in the passenger cabin of a BAe 748 with (b) and without (a) active noise control. (After Elliott *et al.*, 1990).

coefficient, α, which can be used in eqn. (42) to a value which is inversely proportional to this delay (Elliott *et al.*, 1987). Hence the bandwidth, over which the gain of the feedback loop, eqn. (43), is high, will also be limited. The bandwidth over which significant disturbance attenuation can be achieved is thus of the order of the inverse of the plant delay.

As well as controlling tonal disturbances, the Multiple Error LMS algorithm can be used for MIMO control of random disturbances if a set of suitable reference signals is available. The most widely studied example of feedforward active control for random disturbances is the control of random noise in ducts, for which an upstream detection microphone can be used to provide a convenient reference signal (Eriksson *et al.*, 1987). Another example is the control of road noise in cars, where the reference signals in this case are derived from accelerometers on the car body and give time-advanced information about sound inside the car when driving over rough roads. The performance of such a multichannel feedforward control system can be predicted from the exact least-squares solution to eqn. (41). This least squares solution has been used with a set of measured data taken from six accelerometers and a microphone in a car to predict the performance of such a feedforward system, with the result shown in Fig. 19 (Elliott and Sutton, 1996; Sutton *et al.*, 1994). Reductions of up to 10 dB are predicted over a frequency range from about 50 Hz to 200 Hz. The plant response in these calculations has been assumed to have a delay of either 1 ms or 5 ms, and it can

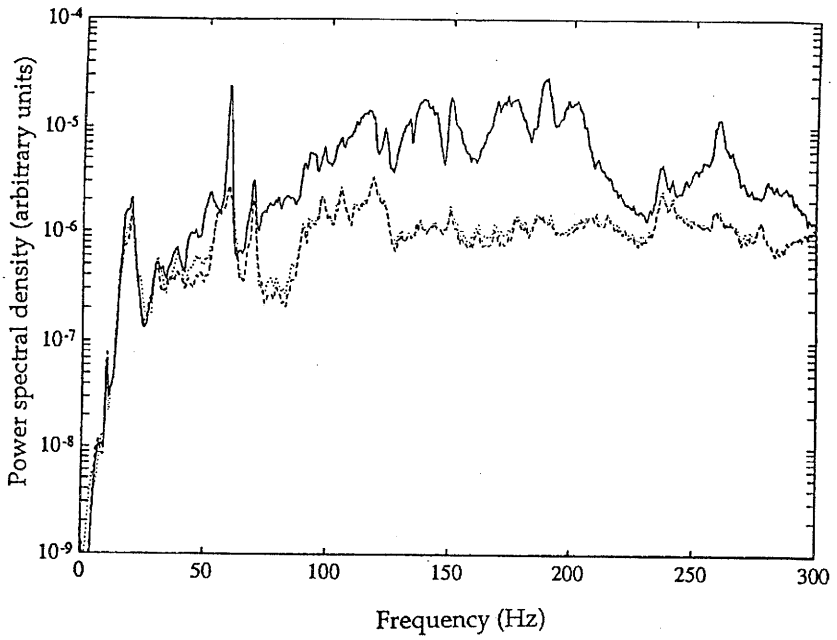

Fig. 19. *A*-weighted power spectral density of the pressure measured in a car (solid line) and the predicted level of the residual spectrum after feedforward control operating with a plant delay of 1 ms (dashed line) or 5 ms (dotted line).

be seen that the performance of the feedforward controller is not significantly affected by plant delays in this range. An adaptive real time controller using the Multiple Error LMS algorithm was also implemented in this investigation and was found to give a performance very close to that shown in Fig. 19. For stochastic disturbances the adaptive feedforward controller does not have an obvious equivalent feedback interpretation, since the reference signals are supplying time-advanced information.

5. Adaptive Feedback Control

5.1. Internal Model Control

It is often the case that no prior knowledge or time-advanced information can be obtained for a stochastic disturbance. The disturbance may be generated, for example, by many individual primary sources at different positions in space, each operating independently. Boundary layer noise in aircraft is an example of this, where the disturbance is created by many small and incoherent eddies convecting past the outside of the aircraft fuselage. Under these conditions a feedback control system can be used for active control, as illustrated for the multichannel case in Fig. 20(a).

In order to contrast the performance of such a feedback system in controlling random noise with that of the feedforward controller discussed above, we will consider the Internal Model Control, IMC, architecture of controller (as described e.g. by Morari and Zafiriou, 1989), which is illustrated in Fig. 20(b). The use of this architecture in the analysis of feedback control systems can be traced back to Newton *et al.* (1957), and it is also known as Youla Parameterisation (Youla *et al.*, 1976) or Q parameterisation (Boyd and Barratt, 1991). In this arrangement an internal model of the plant $\hat{\boldsymbol{G}}$ is used to extract an estimate, $\boldsymbol{x}$, of the disturbance from the error signal, and this is "fed forward" via the control filter $\boldsymbol{W}$ to the plant. If we assume for the moment that the plant model is perfect, $\hat{\boldsymbol{G}} = \boldsymbol{G}$, then the system becomes purely feedforward as shown in Fig. 20(c) and the time domain formulation presented above can directly be used to calculate the optimum least-squares performance for a given disturbance and a given plant response. The difference now is that instead of the performance being dependent on the cross-correlation between the disturbance and the reference signal, as in the feedforward case, the performance depends only on the autocorrelation function of the disturbance signal. If the plant, $\boldsymbol{G}$, contains a pure delay, for example, it is clear that the control filter $\boldsymbol{W}$ must act as a predictor for the disturbance.

Figure 21 shows an example of such a performance calculation using the same road noise data as was used for demonstrating the performance of the feedforward controller in Fig. 19 (Elliott and Sutton, 1996). In this case, however, no separate reference signals were taken into account, but the measured pressure signal was used as both an error signal and a reference signal in the IMC arrangement shown in Fig. 20(b). The plant response was again assumed to be a pure delay of either 1 ms or 5 ms, and in this case the different plant delays produce a significantly different result. With a plant delay of 1 ms the residual spectrum after control is almost flat, indicating that all the predictable components have been removed and the residual

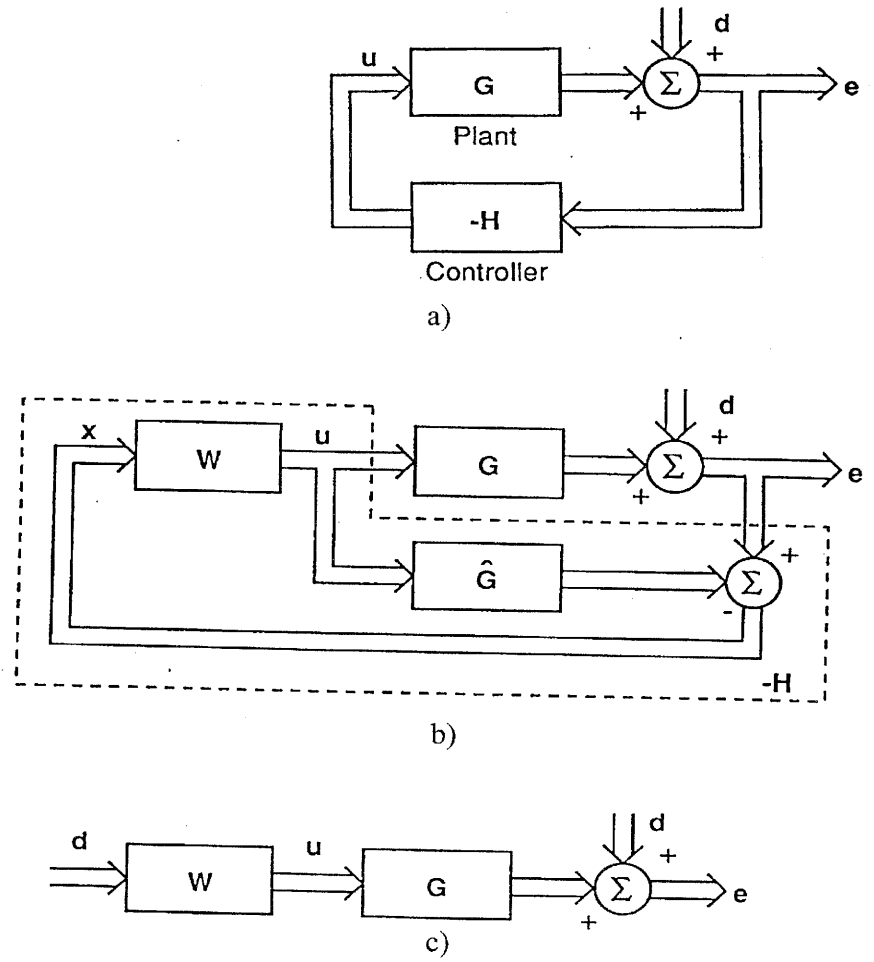

Fig. 20. Block diagram of a multichannel feedforward controller in direct form (a), using internal model control (b) and the equivalent feedforward block diagram if the plant model is perfect (c).

error is uncorrelated over this bandwidth. With a 5 ms plant delay the residual spectrum is more coloured but still smoother than the original disturbance, indicating that the control filter cannot predict the disturbance signal with any accuracy over a timescale of 5 ms.

Internal Model Control thus provides a common formulation within which the performance of feedforward and feedback controllers can be compared. Figure 22, for example, shows the overall attenuation in mean-square level of the A-weighted pressure calculated, for various plant delays, with the road noise disturbance using either a feedforward system, with six reference signals derived from accelerometers on the body, or a feedback system, with only an internal reference signal (Elliott and

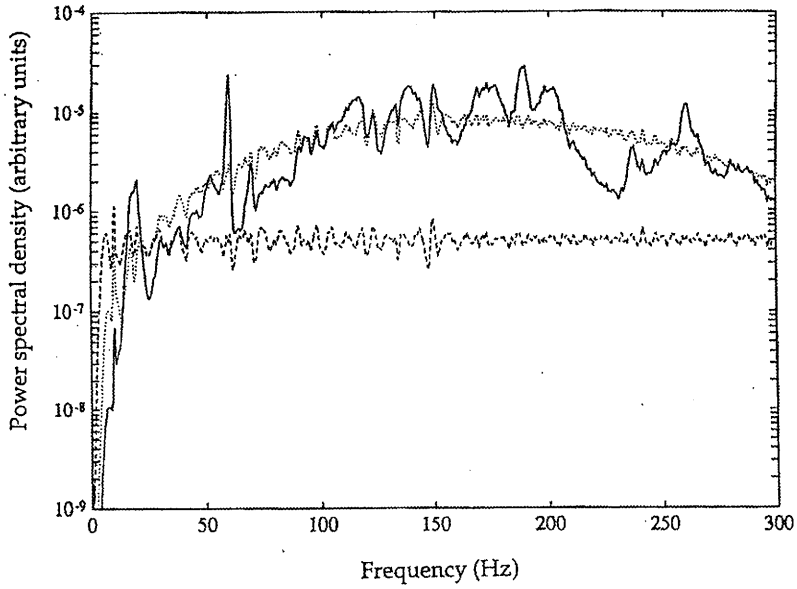

Fig. 21. *A*-weighted power spectral density of the pressure measured in a car (solid line) and the predicted level of the residual spectrum after feedback control operating with a plant delay of 1 ms (dashed line) or 5 ms (dotted line).

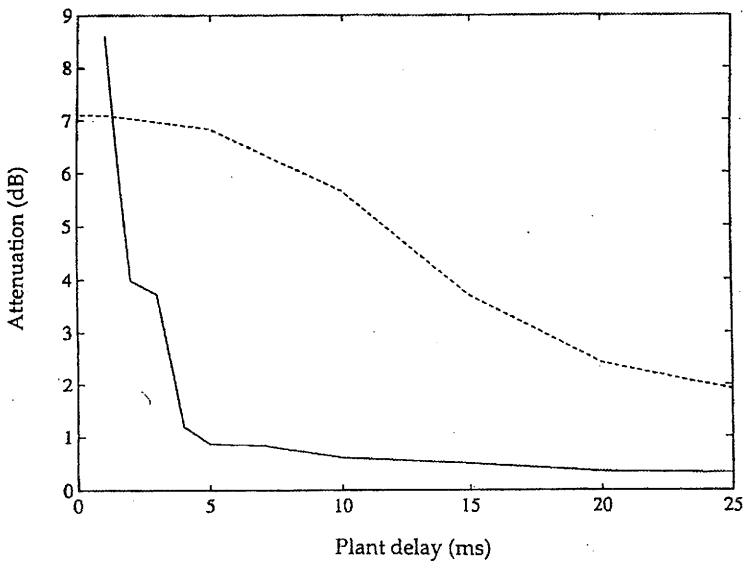

Fig. 22. The variation of the attenuation of the mean square value of the *A*-weighted pressure with plant delay for a feedforward control system (dashed line) and feedback control system (solid line).

Sutton, 1996). The prior information available to the feedforward controller makes its performance relatively insensitive to plant delays of up to 5 ms, whereas the feedback controller can hardly achieve any overall attenuation for such a plant delay. The feedback controller does perform better than the feedforward controller for plant delays of less than about 1.5 ms, however. It should be noted that such a small delay would require the error microphone to be positioned close to a secondary loudspeaker, since the acoustic propagation delay is about 3 ms/metre in air, which would restrict the spatial extent of the zone of quiet which could be achieved, as described in Section 2. Also, the feedback system would attenuate all the sound in the car within its bandwidth, potentially including speech and warning signals. The feedforward system has the advantage that it is selective in that it will only control the sound which is correlated with the external reference signals, the road noise in this case.

It is thus clear that in active sound control applications, where disturbance rejection is most important, both the optimum controller and the optimum performance will depend not only on the non-minimum phase characteristics of the plant but also on the autocorrelation properties of the disturbance, which are largely determined in this case by the autocorrelation properties of the primary sources. In applications where the disturbance is non-stationary the controller must thus be adaptive to maintain optimum performance even if the plant response does not change. The IMC architecture provides a convenient framework within which to design such an adaptive controller, as discussed in Section 5.3.

In active vibration control systems, however, the structure under control is usually highly resonant, as discussed in Section 2, and the disturbance is generated by the primary source acting on this structure. The disturbance is heavily influenced by the resonances of the structure under control and becomes more predictable, and thus easier to control with a feedback controller, as a result of these resonances. The performance of many active vibration control systems is less dependant on the autocorrelation properties of the primary sources than is the performance of many active sound control systems, since the autocorrelation structure of the disturbance is dominated by the response of the system under control. It is a common assumption in the analysis of feedback control systems that the plant and the disturbance model share the same poles. Whereas this is a reasonable assumption for most active vibration control systems, where the plant dynamics and autocorrelation structure of the disturbance are dominated by the resonances of the structure under control, it is often not a reasonable assumption for active sound control systems, in which the plant response is dominated by the dynamics of the secondary actuator and the electroacoustic delay, and the acoustic environment has a relatively small effect on the autocorrelation function of the disturbance.

5.2. Robustness

An obvious danger with the IMC architecture shown in Fig. 20b is that of instability if the response of the plant model $\hat{\boldsymbol{G}}$ is not equal to that of the plant $\boldsymbol{G}$. Although with a perfect plant model the system is effectively feedforward, and thus stable for all stable control filters, $\boldsymbol{W}$, a control filter with a high gain could combine together with

a small plant modelling error to cause instability. Fortunately, the stability robustness of a feedback controller to changes in plant response has been widely studied in recent years (see e.g. Doyle *et al.*, 1992; Maciejowski, 1989; Morari and Zafiriou, 1989) and some of this knowledge can be directly applied in this case. If we assume that the plant model was initially perfect for some nominal plant, so that $\hat{\boldsymbol{G}} = \boldsymbol{G}_0$, but that the plant response is then subject to unstructured multiplicative output uncertainty, so that

$$\boldsymbol{G}(j\omega) = \Big[\boldsymbol{I} + \Delta_G(j\omega)\Big]\boldsymbol{G}_0(j\omega) \tag{45}$$

where the largest singular value of $\Delta_G j\omega)$ is bounded by

$$\bar{\sigma}\Big[\Delta_G(j\omega)\Big] < B(\omega) \tag{46}$$

and $B(\omega)$ is the upper bound on the uncertainty, then the condition for robust stability is that (Morari and Zafiriou, 1989),

$$\bar{\sigma}\Big[\boldsymbol{T}_0(j\omega)\Big] < \frac{1}{B(\omega)} \quad \text{for all } \omega \tag{47}$$

where $\boldsymbol{T}_0(j\omega)$ is the complementary sensitivity function, which for the conventional feedback controller shown in Fig. 20(a) is

$$\boldsymbol{T}_0(j\omega) = \boldsymbol{G}_0(j\omega)\boldsymbol{H}(j\omega)\Big[\boldsymbol{I} + \boldsymbol{G}_0(j\omega)\boldsymbol{H}(j\omega)\Big]^{-1} \tag{48}$$

If an IMC architecture of feedback controller is used, as in Fig. 20(b), then the complementary sensitivity function is equal to the simpler expression,

$$\boldsymbol{T}_0(j\omega) = \boldsymbol{G}_0(j\omega)\boldsymbol{W}(j\omega) \tag{49}$$

and the condition for robust stability becomes

$$\bar{\sigma}\Big[\boldsymbol{G}_0(j\omega)\boldsymbol{W}(j\omega)\Big] < \frac{1}{B(\omega)} \quad \text{for all } \omega \tag{50}$$

or

$$\Big\|\boldsymbol{G}_0(j\omega)\boldsymbol{W}(j\omega)B(\omega)\Big\|_\infty < 1 \tag{51}$$

The robust stability condition can thus be seen as a constraint on the control filter $\boldsymbol{W}$ which depends on the frequency response of the plant and the frequency dependence of the multiplicative uncertainty. If the objective were to minimise the maximum spectral component of the error, an H_∞ control requirement (e.g. Doyle *et al.*, 1992) may be

$$\text{minimise } \Big\|\boldsymbol{e}(j\omega)\Big\|_\infty \text{ subject to } \Big\|\boldsymbol{G}_0(j\omega)\boldsymbol{W}(j\omega)B(\omega)\Big\|_\infty < 1 \tag{52}$$

In the case of active sound and vibration control we are generally interested in minimising the mean square value of the error, since this is proportional to the perceived

sound level, and thus to achieve this objective while maintaining robust stability the controller requirements become

$$\text{minimise} \left\| \boldsymbol{e}(j\omega) \right\|_2 \text{ subject to } \left\| \boldsymbol{G}_0(j\omega)\boldsymbol{W}(j\omega)B(\omega) \right\|_\infty < 1 \tag{53}$$

which is a mixed H_2/H_∞ problem, considered e.g. by Titterton and Olkin (1995) and Rafaely and Elliott (1996a).

There are some difficulties in solving eqn. (53) directly and so we have also investigated the related quadratic problem, whose solution can be readily found, of minimising the cost function J given by

$$\text{minimise } J = \left\| \boldsymbol{e}(j\omega) \right\|_2^2 + \beta \left\| \boldsymbol{G}_0(j\omega)\boldsymbol{W}(j\omega)B(\omega) \right\|_2^2 \tag{54}$$

which could be called "robust H_2 control." It is interesting to note how this cost function is similar to, but not the same as, that described in Section 4 which included mean square control effort with mean square error. Parseval's theorem can be used to write this quadratic cost function in the time domain and it can be analytically minimised for various values of the parameter β (Elliott and Sutton, 1996). The optimum solution for each value of β gives a different compromise between performance, i.e. the minimum value of $\|\boldsymbol{e}\|_2^2$, and robustness, i.e. the value of $B(\omega)$ for which $\|\boldsymbol{G}_0(j\omega\boldsymbol{W}(j\omega)B(\omega)\|_\infty < 1$. This variety of compromise solutions is plotted in Fig. 23 for the example of the road noise data with a plant delay of 1 ms and a frequency independent multiplicative uncertainty. For small values of β, more than 8 dB of overall attenuation of the mean square signal can be obtained, but the system is only robustly stable for fractional plant uncertainties of less than about 6%, which corresponds to 0.5 dB gain variation or 3.5° phase variation. In order to make the feedback controller robust to fractional plant uncertainties of 33%, i.e. 2.5 dB gain or 20° phase variation, β must be increased until the attenuation in mean square value is only about 6 dB. By iteratively adjusting $B(\omega)$ so that at each iteration it is proportional to $\boldsymbol{G}_0(j\omega)\boldsymbol{W}(j\omega)$, higher powers of $\|\boldsymbol{G}_0(j\omega)\boldsymbol{W}(j\omega)B(\omega)\|_2$ in eqn. (54) can be minimised by iterative quadratic optimisation (Elliott and Sutton, 1996; Rafaely and Elliott, 1996b; 1996c). The dotted line in Fig. 23, for example, shows the result of minimising

$$J = \left\| (j\omega) \right\|_2^2 + \beta \left\| \boldsymbol{G}_0(j\omega)\boldsymbol{W}(j\omega)B(\omega) \right\|_4^4 \tag{55}$$

for various values of β. By raising the final term in eqn. (55) to higher powers, the robust stability limitation becomes 'harder' as it tends towards the H_∞ constraint, given by eqn. (53). In this example, where the plant response is pure delay, the resultant compromise between performance and robustness which results from minimising eqn. (55) is not very different from that obtained from the robust H_2 formulation, eqn. (54). Current work is focused on investigating how general this observation may be (Rafaely and Elliott, 1996a).

It has already been observed in Section 4 that the inclusion of an effort weighting term in the cost function being minimised ensures the robust stability of an adaptive feedforward control system. In this section a modified form of effort weighting has been developed which ensures the robust stability of a fixed feedback control system

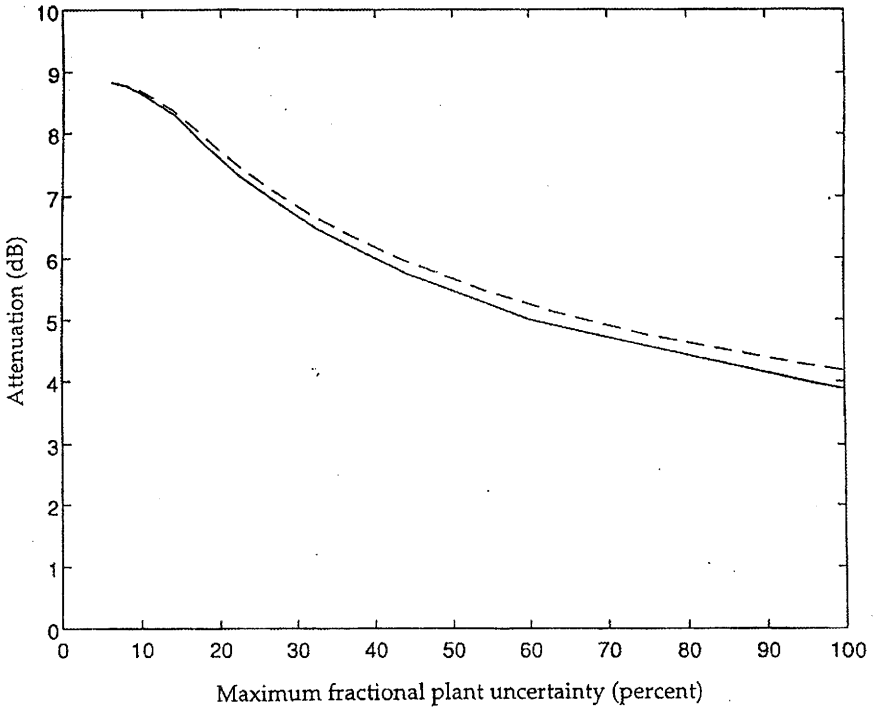

Fig. 23. Variation of the attenuation of the mean square disturbance signal with the maximum fractional plant uncertainty ($B_{\max}$) for robust stability, as the parameter β is varied in (54), solid line, and (55) dashed line.

when a purely quadratic cost function is minimised in the time domain. This cost function will be used in the following section to ensure that when the controller is being adapted it always remains robustly stable.

5.3. Adaptation

It is clear from the discussion above that the optimum performance of a feedback controller depends on both the statistical properties of the disturbance and on the plant response. The IMC architecture provides a convenient framework within which the feedback controller can be made independently adaptive to each of these changes in the system under control. If we assume that the plant response does not change significantly, then it is only the control filter which has to be adapted to cope with a non-stationary disturbance, as illustrated in Fig. 24(a). Because the system is now essentially feedforward, the time domain adaptation algorithms discussed in Section 4 can now be used to adjust the control filter $\boldsymbol{W}$. In practice, however, the plant model will never be perfect and/or the plant response is bound to change to some extent. The control filter must then be adapted so that it is always robustly stable. A relatively simple modification to the time domain LMS algorithm has been developed which

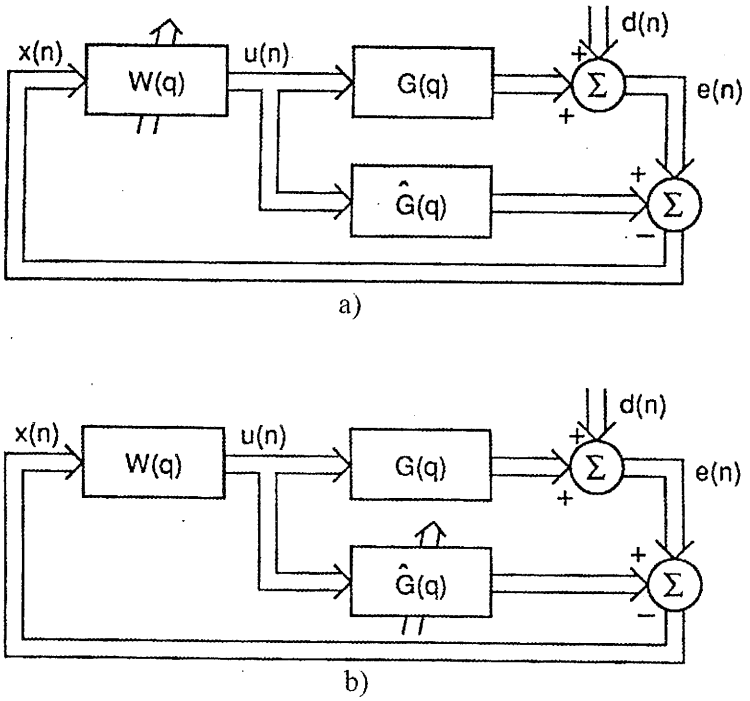

Fig. 24. Block diagram of an IMC feedback controller adapted to track a non-stationary disturbance (a) and a time-varying plant response (b).

incorporates the quadratic robust stability term of eqn. (54) and this has proved to be successful in adapting robust feedback controllers to track non-stationary disturbances (Rafaely and Elliott, 1996b). Adaptive algorithms operating in the frequency domain which converge to a least square optimal filter within the robust stability constraint, and thus approach the solution to the H_2/H_∞ problem defined by eqn. (53), have also recently been suggested (Elliott and Rafaely, 1997).

If the changes in the plant response become too large, then even though the system can still be made robustly stable, the performance will be severely degraded. Under these conditions it may be preferable to use the adaptive controller shown in Fig. 24(b), in which the plant model is adapted to track the changes in the plant response (Rafaely and Elliott, 1996b). In order to adapt the plant model, it is generally necessary to inject identification noise into the plant, and if the level of this noise is too high in an active sound control system the resultant acoustic noise can be louder than it was without control! The level of the identification noise must thus generally be somewhat below that of the residual error, although the level of identification noise could be scheduled on the measured error (Wright, 1988) or the spectrum of the identification noise could be tailored such that it was least objectionable (Coleman and Berkman, 1995). If both the control filter and the plant model are adapted over

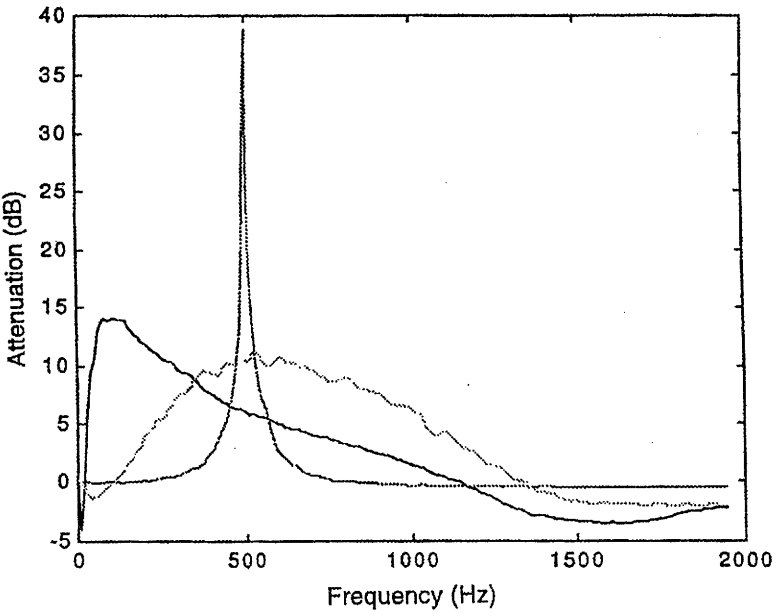

Fig. 25. Disturbance attenuation of an active headset with a fixed analogue controller (solid line) and an adaptive digital controller after convergence with a broad-band disturbance (feint line) or a tonal disturbance (dotted line).

similar time frames there can be significant interaction between the two adaptive processes. One solution to this, which has been successfully implemented in practise, is to 'freeze' the response of one filter while the other is being adapted. Generally though, the restriction on the level of the identification noise limits the adaptive plant identification to the tracking of relatively slow drifts in the plant response, and more rapid variations in plant response must be dealt with by making the feedback controller robust to these plant uncertainties.

As an example of the performance which can be obtained from a robust, disturbance-adaptive feedback controller, Fig. 25 shows the sound attenuation measured in a commercial open-backed active headset with the fixed analogue controller, as supplied, and with an adaptive digital filter after it had converged in two different noise fields (Rafaely and Elliott, 1996b). The fixed analogue controller gives good attenuation from about 50 Hz to 500 Hz, which is generally the frequency region over which the listener would want to attenuate noise in an aircraft for example. The digital controller was adapted to minimise the mean square error at the microphone when the disturbance spectrum was either a band of noise centred on 500 Hz, or a pure tone at 500 Hz. By using the modified form of the time domain LMS algorithm to adapt the control filter, the robustness of the adaptive controller was constrained to be no worse than that of the original analogue controller. Clearly the adaptive controller is able to give a better performance for these types of disturbances than

the fixed analogue controller and is also able to track changes in the disturbance spectrum. The active headset is a rather severe test for an adaptive feedback system since the plant frequency response, from headset loudspeaker to close-spaced microphone, can increase in amplitude by up to 10 dB over very short timescales, as the headset is adjusted on the listener's head. It is difficult to track these very rapid changes with a plant identification scheme using an acceptable level of identification noise, and so in this case the control filter is adapted using an algorithm which made the stability of the resulting feedback controller very robust to plant uncertainty.

6. Conclusions

The successful application of active methods in controlling noise and vibration requires an understanding of both its physical limitations and its electrical realisation. The physical limitations are determined by the fact that the spatial variation of the disturbance is governed by a wave equation and so are limited by the wavelength of the disturbance in the system under control. This may be the flexural wavelength for the control of vibration on a plate or the acoustic wavelength for the control of sound in an enclosure. Provided the system under control is not too heavily damped or too large compared with this characteristic wavelength, then it is generally possible to achieve global control of the system, i.e. reduce its total energy, with a reasonable number of secondary actuators. Even if global control is not possible, a zone of quiet can still be created close to the secondary actuator, although its dimensions will be relatively small compared with the wavelength.

The control problems associated with active attenuation are rather different from those encountered in many control systems. This is partly due to the nature of the plant response in this case which, particularly for active sound control systems, (a) have very little resonant behaviour, (b) have considerable propagation delay compared with the periods of the disturbances being controlled, and (c) generally have a number of d.c. zeros. These acoustic plant responses also tend to be subject to rapid variations, as people move around within an enclosure for example. In many of the applications of active control, the low frequency disturbances are almost periodic and of known frequency. Thus feedforward control techniques, which were originally developed for controlling sound propagating along ducts, are very prevalent. In order to track non-stationarities in the disturbance the feedforward controllers are typically made adaptive. Modern systems use adaptive digital filters and it has been shown that for a harmonic reference signal such adaptive feedforward controllers behave in exactly the same way as fixed feedback systems. This suggests that the design of such controllers could benefit from the theoretical formulations which have been widely used for multichannel feedback control systems, particularly with regard to their robustness in the face of plant uncertainty.

For a random disturbance, if the location of the original source of the noise or vibration is well defined, it may still be possible to use feedforward techniques in the active control system. Certainly any advance knowledge of the disturbance can significantly improve the ultimate attenuation achieved. In an example of controlling

road noise in a car, for example, a feedforward controller was able to give significantly more attenuation than a feedback controller for realistic plant delays.

By considering the Internal Model Control, IMC, architecture for a feedback controller, a consistent treatment of the control problem can be formulated across both feedforward and feedback control systems. The IMC architecture also allows a relatively simple interpretation of the robust stability limit of a practical controller. It has been shown how this robust stability limit can be improved by the minimisation of a purely quadratic cost function, and that the resulting trade-off between performance and robustness is quite similar, in an example application, to that which could be achieved using a harder robust stability limitation, which approximates the H_∞ constraint.

Finally, the IMC arrangement also motivates the design of an adaptive feedback controller, which has two separate adaptation processes to maintain optimal performance for either a non-stationary disturbance or a time-varying plant. The adaptation can be achieved in the time domain while maintaining a specified level of robust stability.

References

Boyd S.P. and Barratt C.H. (1991): *Linear Controller Design, Limits of Performance.* — Prentice Hall.

Coleman R.B. and Berkman E.F. (1995): *Probe shaping for on-line plant identification.* — Proc. *Active'95*, Newport Beach, pp.1161–1170.

Conover W.B. (1956): *Fighting noise with noise.* — Noise Control Vol.2, pp.78–82.

Doyle J.C. *et al.* (1992): *Feedback Control Theory.* — MacMillan.

Elliott S.J. *et al.* (1987): *A multiple error LMS algorithm and its application to the active control of sound and vibration.* — IEEE Trans. Acoustics, Speech and Signal Proc. ASSP–35, pp.1423–1434.

Elliott S.J. *et al.* (1988a): *Active cancellation at a point in a pure-tone diffuse soundfield.* — J. Sound Vibr., Vol.120, pp.183–189.

Elliott S.J. *et al.* (1988b): *The active control of engine noise inside cars.* — Proc. *Inter-Noise'88*, pp.987–990.

Elliott S.J. *et al.* (1990): *In-flight experiments on the active control of propeller-induced cabin noise.* — J. Sound Vibr., Vol.140, pp.219–238.

Elliott S.J. *et al.* (1992): *The behaviour of a multiple channel active control system.* — IEEE Trans. Acoustics, Speech and Signal Proc. ASSP–40, pp.1041–1052.

Elliott S.J. and Nelson P.A. (1993): *Active noise control.* — IEEE Signal Proc. Mag., pp.12–35.

Elliott S.J. and Sutton T.J. (1996): *Performance of feedforward and feedback systems for active control.* — IEEE Trans. Speech and Audio Proc., Vol.4, pp.214–223.

Elliott S.J. and Rafaely B. (1997): *Frequency domain adaptation of feedforward and feedback controllers.* — Proc. *Active'97*, Budapest.

Eriksson L.J. *et al.* (1987): *The selection and application of an IIR adaptive filter for use in active sound attenuation.* — IEEE Trans. Acoustics, Speech and Signal Proc. ASSP–35, pp.433–437.

Franklin G.F. *et al.* (1990): *Digital Control of Dynamic Systems (2nd Ed.).* — Addison-Wesley.

Fuller C.R. *et al.* (1996): *Active Control of Vibration.* — London: Academic Press.

Garcia-Bonito J.J. and Elliott S.J. (1996): *Local active control of vibration in a diffuse bending wave field.* — ISVR Techn. Memorandum, No.790.

Haykin S. (1996): *Adaptive Filter Theory, 3rd Ed.* — Prentice Hall.

Johnson M.E. and Elliott S.J. (1995): *Experiments on the active control of sound radiation using a volume velocity sensor.* — Proc. *SPIE Conf.*, Vol.2443, pp.658–668.

Lueg, P. (1936): *Process of silencing sound oscillations.* — US Patent No.2, 043, 416.

Maciejowski J.M. (1989): *Multivariable Feedback Design.* — Addison-Wesley.

Morari M. and Zafiriou E. (1989): *Robust Process Control.* — New Jersey: Prentice Hall.

Morgan D.R. (1980): *An analysis of multiple correlation loops with a filter in the auxiliary path.* — IEEE Trans. Acoustics, Speech and Signal Proc. ASSP–28, pp.454–467.

Morgan D. and Sanford C. (1992): *A control theory approach to the stability and transient response of the filtered-x LMS adaptive notch filter.* — IEEE Trans. Signal Proc. SP–40, pp.2341–2346.

Nelson P.A. and Elliott S.J. (1992): *Active Control of Sound.* — London: Academic Press.

Press W.H. *et al.* (1986): *Numerical Recipes.* — Cambridge: Cambridge University Press.

Newton G.C., Gould L.A. and Kaiser J.F. (1957): *Analytical Design of Feedback Controllers.* — New York: Wiley.

Rafaely B. and Elliott S.J. (1996a): *H_2/H_∞ active control of sound: Design formulation, solution and implementation.* — IEEE Trans. Contr. Syst. Techn., (in print).

Rafaely B. and Elliott S.J. (1996b): *Adaptive plant modelling in an internal model controller for active control of sound and vibration.* — Proc. Conf. *Identification in Engineering Systems*, University of Wales, pp.479–488.

Rafaely B. and Elliott S.J. (1996c): *An adaptive and robust controller for active control of sound and vibration.* — Proc. *CONTROL'96*, Exeter, No.427, pp.1149–1153.

Sievers L.A. and von Flotow A.H. (1992): *Comparison and extension of control methods for narrowband disturbance rejection.* — IEEE Trans. Signal Proc. SP–40, pp.2377–2391.

Sutton T.J. *et al.* (1994): *Active control of road noise inside vehicles.* — Noise Contr. Eng. J., Vol.42, pp.137–147.

Titterton P.J. and Olkin J.A. (1995): *A Practical method for constrained-optimisation controller design: H_2 or H_∞ optimisation with multiple H_2 or H_∞ constraints.* — Proc. 29th IEEE Asilomar Conf. *Signals, Systems and Computers*, pp.1265–1269.

Widrow B. and Stearns S.D. (1985): *Adaptive Signal Processing.* — New Jersey: Prentice Hall.

Widrow B. and Hoff M. (1960): *Adaptive switching circuits.* — Proc. Ire Westcon, pt.4, pp.96–104.

Wright M. (1988): *Active control in changing environments.* — B. Sc. Project Dissertation, University of Southampton.

Youla D.C. *et al.* (1976): *Modern Wiener–Hopf design of optimal controllers, Part 1: The single channel case.* — IEEE Trans. Automat. Contr., Vol.AC21, pp.3–13.